CO_2-rich rejuvenated volcanic rocks on Hawaiian islands

Guoliang Zhang[1,2,3*], Shuai Wang[1], Shichun Huang[4], Mingjun Zhan[1], Junhua Yao[1]

[1] Center of Deep Sea Research & Key Laboratory of Marine Geology and Environment, Institute of Oceanology, Chinese Academy of Sciences, Qingdao 266071, China

[2] Laboratory for Marine Geology, Qingdao National Laboratory for Marine Science and Technology, Qingdao 266000, China

[3] Center for Ocean Mega-Science, Chinese Academy of Sciences, Qingdao 266071, China

[4] Department of Geoscience, University of Nevada, Las Vegas, NV 89154-4010, USA

***Corresponding author:** Guoliang Zhang (zhangguoliang@qdio.ac.cn)

Abstract

Sedimentary carbonates are sent to the deep mantle if they are not completely destroyed at subduction zones, and subducted carbonates may contribute to plume volcanism. To better constrain the role of recycled carbonates in Hawaiian volcanism, we report high-precision olivine and whole-rock geochemical compositions of shield and rejuvenated stage lavas from Kauai, Oahu and Maui islands. The studied rejuvenated stage whole-rocks have low SiO_2 and high CaO concentrations, and are depleted in HFSEs, such as, Nb and Zr, consistent with a role of carbonated melt. Rejuvenated stage olivines have Ni abundance lower than and CaO and MnO contents similar to those of shield stage at a given Fo. The calculated partition coefficients of Ca ($D_{Ca}^{Ol\text{-}melt}$) and Mn ($D_{Mn}^{Ol\text{-}melt}$) between olivine and shield melts are consistent with those of a dry melt system. However, the low $D_{Ca}^{Ol\text{-}melt}$ and $D_{Mn}^{Ol\text{-}melt}$ for rejuvenated lavas can only be explained by a volatile-rich melt system. Based on the observed $D_{Ca}^{Ol\text{-}melt}$ and $D_{Mn}^{Ol\text{-}melt}$ in rejuvenated lavas, and considering the effect of H_2O, our modeling calculation shows that rejuvenated primary magmas contain up to ~10

wt% CO_2. Using olivine-spinel aluminum exchange thermometry, we show that the rejuvenated primary magma temperatures are similar to/slightly lower than those of shield stage. We posit that the lower rejuvenated stage lavas were originated from melting of carbonated peridotites in the plume. The carbonated melts that metasomatized the peridotites were likely derived from subducted ancient carbonate-bearing lithospheric mantle.

Keywords: olivine, CO_2, metasomatism, rejuvenated lavas, mantle plume, Hawaiian islands

1 Introduction

The deep mantle may store most of the Earth's carbon (Dasgupta and Hirschmann, 2006; Dasgupta and Hirschmann, 2010; Zhang et al., 2017; Plank and Manning, 2019). Plate subduction is considered to be an important factor of carbon enrichment in the deep Earth's interior (Dasgupta and Hirschmann, 2010; Plank and Manning, 2019). Deep-rooted mantle plumes (e.g., Hawaiian plume) are good candidate for the study of deep Earth's carbon cycle (Dixon et al., 2008). Since CO_2 can significantly change the chemistry of mantle-sourced melts, e.g., lowing SiO_2 and elevating CaO of melts (Dasgupta et al., 2007a; Foley et al., 2009; Zhang et al., 2017), it may play an important role in the origin of alkali basalts (Dixon et al., 2008; Dasgupta et al., 2006, 2007a&b; Sisson et al., 2009).

The Emperor-Hawaii seamount chain is a type volcanic chain that may originate from near the core-mantle boundary (Montelli et al., 2004; Huang et al., 2011; Weis et al., 2011; French and Romanowicz, 2015). Shield stage tholeiitic basalts account for the majority (95 vol%) of Hawaiian volcanic rocks, while pre-shield, post-shield and rejuvenated stages account for the rest 5% (Sherrod et al., 2007). The role of an olivine-free lithology, pyroxenite or eclogite, in the petrogenesis of Hawaiian shield lavas is highly debated. Specifically, Hawaiian shield tholeiitic lavas have too high SiO_2 content to be produced by partial melting of garnet peridotite (e.g., Hauri, 1996; Wagner and Grove, 1998; Huang and Frey, 2005). This led to the suggestion that an eclogite component play a role in producing the high SiO_2 contents in Hawaiian tholeiitic lavas (Hauri, 1996; Huang and Frey, 2005). Alternatively, the high SiO_2 content may be a result of melt-harzburgite reaction (Wagner and Grove, 1998). Sobolev et al. (2005; 2007) and Herzberg (2006; 2011) noted that the high olivine Ni contents and low CaO and MnO in olivines from

Hawaiian shield lavas, as well as low whole rock CaO contents, required a pyroxenite-dominated mantle source for Hawaiian shield lavas. Alternatively, the low CaO and MnO contents, and high SiO_2 content of Hawaiian lavas may be explained if they represent mixtures of partial melts from garnet peridotite and from eclogite (Huang et al., 2007). Matzen et al. (2013; 2017) showed that the high olivine Ni content in Hawaiian shield stage olivines may simply reflect the temperature difference between partial melting beneath the thick lithosphere and olivine crystallization in a shallow magma chamber, and a pyroxenite-dominated mantle source is not required.

Hawaiian rejuvenated stage volcanism occurred 0.5-2 Myr after shield stage and consists of silica-undersaturated alkaline-rich rocks, e.g., alkali basalt, hawaiite, nephelinite and melilitite (e.g., Clague and Dalrymple, 1987; Garcia et al., 2010; Phillips et al., 2016). Hawaiian rejuvenated lavas are among the most silica-undersaturated and alkaline-rich in oceanic islands/seamounts (Chauvel et al., 1997; Zhang et al., 2020). It remains unclear on the origin of rejuvenated stage low-SiO_2 alkali-rich volcanic rocks (Reiners and Nelson, 1998; Bianco, 2005; Garcia et al., 2010; Ballmer, 2011; Hofmann and Farnetani, 2013; Phillips et al., 2016). Hawaiian rejuvenated lavas are more depleted in Sr-Nd-Hf isotope compositions than those of shield stage (e.g., Chen and Frey, 1983; Frey et al., 2000; 2005 G-cubed; Yang et al., 2003; Hofmann and Farnetani, 2013; Beguelin et al., 2019; DeFelice et al., 2019; Harrison et al., 2020), indicating different mantle sources. Earlier studies suggested an origin of Hawaiian rejuvenated lavas from the underlying metasomatically enriched Pacific lithospheric mantle (Chen and Frey, 1983; Garcia et al., 2010). However, there are increasing studies suggesting the isotopically depleted rejuvenated stage source component is intrinsic of the mantle plume (Ribe and Christensen, 1999 EPSL 171, 517-531; Hofmann and Farnetani, 2013; DeFelice et al., 2019; Harrison et al., 2020; but see also Beguelin et al., 2019 for a different opinion).

Silica under-saturated alkali lavas could be explained by involvement of CO_2 in the mantle source (Mallik and Dasgupta, 2012; 2013). Several studies have indicated that CO_2 played an important role in the origin of Hawaiian lavas (Dixon et al., 2008; Huang et al., 2009&2011; Sisson et al., 2009; Borisova and Tilhac, 2021). Tucker et al (2019) showed that the mantle sources of Hawaiian shield stage lavas contain 380-480 ppm CO_2 based on measurement of olivine hosted melt inclusions, while the source CO_2 contents of rejuvenated lavas were not constrained. Dixon et al (2008) explained Hawaiian rejuvenated lavas with elevated Ba/Th by

carbonatite metasomatism, but the content of CO_2 has not been directly constrained. CO_2 not only affects magma chemical compositions, but also element partitioning between olivine and melts (Gavrilenko et al., 2016). Gavrilenko et al (2016) proposed that magma CO_2 concentration could be calculated based on its influence on Ca partition between olivine/melt. In this study, we have analyzed high-precision olivine chemistry and whole-rock major and trace elements of Hawaiian rejuvenated stage lavas, aiming to evaluate the role of CO_2 in Hawaiian magmatism.

2 Samples

Shield and rejuvenated stage rock samples in this study were collected from Kauai, Oahu and Maui Islands (Fig. 1), and their information is in Supplementary Table 1. We have collected 26 rock samples, including 16 rejuvenated stage and 10 shield stage, from these islands (Fig. 1; Supplementary Table 1). At Kauai Island, there are two sampling sites from the shield stage Waimea volcanics (5.5-4 Ma), and 5 sites from the rejuvenated stage Koloa volcanics (2.6-0.15 Ma). At Oahu Island, there are 2 sampling sites from the shield stage Wai'anae volcanics and 1 site from the shield stage Ko'olau volcano (3.0-1.8 Ma); 2 sampling sites from the rejuvenated stage Honolulu volcanics (0.8-<0.1 Ma). At Maui Island, there is 1 sampling site from the shield stage Wailuku volcanics (2.0-1.3 Ma); 2 sites from the rejuvenated stage Hana volcanics (0-1.5 Ma) and 1 site from the rejuvenated stage Kula volcanics (0.93-0.15 Ma). The detailed information on division of volcanics can be referred to Sherrod et al (2007). Despite the absence of distinct differences in formation age between the Hana and Kula volcanics, we classify the Hana and Kula volcanics as rejuvenated stage because of their low-silica and high alkaline characteristics. The detailed information on sampling can be found in Supplementary Table 1.

3 Methods and results

3.1 Methods

The 26 rock samples were analyzed for bulk-rock major and trace elements, and their olivine phenocrysts were analyzed for major and trace elements using in situ high-precision Electron Probe Microanalyzer (EMPA) technique. Bulk-rock major elements were analyzed using fused glass discs with an Axios sequential X-ray Fluorescence Spectrometer at Institute of Geology and Geophysics, Chinese Academy of Sciences (IGGCAS), Beijing, China. Samples were fused

at 1050 °C using a lithium tetraborate flux ($Li_2B_4O_7$) in a mixture consisting of 0.5 g of sample and 5 g of lithium tetraborate. Loss on ignition (LOI) was determined at a temperature of 1000°C in air for 3 hours. Basalt standards BCR-2, BHVO-2 and GSR-3 were analyzed as unknowns and the results are shown in Supplementary Method Table 1. Bulk-rock trace elements were analyzed by a Perkin-Elmer Sciex ELAN DRC-e ICP-MS at the State Key Laboratory of Ore Deposit Geochemistry (SKLODG), Institute of Geochemistry, Chinese Academy of Sciences (IGCAS). The powdered samples (50 mg) were dissolved with HF + HNO_3 mixture in high-pressure Teflon Bombs at ~190 °C for 48 h (Qi et al., 2000). Rh was used as an internal standard to monitor sensitivity drift during measurement. How do you measure the trace element abundances? BCR-2 and BHVO-2 solutions were used to monitor analytical accuracy. The analytical precision was generally better than 10 % (2 sigma) based on replication of basalt standards analyses.

Quantitative *in situ* analyses of olivine and spinel major and minor elements were conducted on JXA-8230 EMPA equipped with 5 wavelength dispersive spectrometers at Institute of Oceanology, Chinese Academy of Sciences. The operating conditions were: 20 kV accelerating voltage, 60 nA beam current, and 1-5 μm beam diameter. For olivine analyses, the counting time was 30 seconds for Si kα, Mg kα and Fe kα, and 80 seconds for Mn kα, Ni kα, Ca kα, Cr kα, Al kα. The off peak counting time was 80 seconds for Mn kα, Ni kα, Ca kα, Cr kα, Al kα. Standards used were olivine (Si, Mg), corundum (Al), MnO (Mn), wollastonite (Ca), NiO (Ni), and apatite (P), magnetite (Fe), and Cr_2O_3 (Cr). For spinel analyses, the counting time was 30 seconds for Si kα, Mg kα, Al kα, Mn kα, Ni kα, Cr kα, Ti kα and Fe kα. The off peak counting time was 20 seconds for Si kα, Mg kα, Al kα, Mn kα, Ni kα, Cr kα, Ti kα and Fe kα. Standards used were spinel (Al, Mg), quartz (Si), MnO (Mn), rutile (Ti), NiO (Ni), magnetite (Fe) and Cr_2O_3 (Cr). Unknown and standard intensities were corrected for dead time. All data were corrected with the standard ZAF correction procedures. The olivine standard MongOLSh11-2 (Batanova et al., 2019) was replicated during the analyses to monitor the reproducibility and accuracy, and the results are shown in Supplementary Method Table 3.

3.2 Results

3.2.1 Whole-rock major and trace elements

Whole-rock major and trace element compositions are shown in Supplementary Table 2. As

shown in the plot of TAS vs. SiO_2 (Supplementary Fig. 1), shield stage lavas are tholeiitic basalts with two plotting close to the division line between alkali basalt and tholeiitic basalts. Shield stage lavas have SiO_2 between 46.4-50.0 wt%, MgO between 11.5-23.4 wt%，CaO between 5.1-10.7 wt%, Na_2O between 1.44-2.51 wt%, and P_2O_5 between 0.18-0.35 wt%. Shield stage lavas show slight enrichment of light over heavy rare earth elements (REEs) and slight enrichment of Ba. Rejuvenated stage lavas are all rich in alkaline elements and can be classified into foidite, basanite and alkali basalts (Supplementary Fig. 1), of which the three foidite samples from Site O7 (Honolulu volcanics) have the highest alkaline (Na_2O+K_2O) and P_2O_5 and the lowest SiO_2 contents (Fig. 2). Except for Site O7 foidite samples, the other rejuvenated stage samples have SiO_2 between 37.7-45.3 wt%, MgO between 7.15-15.1 wt%, CaO between 9.4-13.3 wt%, Na_2O between 2.4-3.8 wt% and P_2O_5 between 0.33-0.92 wt%.

These rejuvenated stage lavas are strongly enriched in light rare earth elements (LREEs) and large ion lithophile elements (LILEs) (Fig. 3) compared with shield stage lavas. These rejuvenated stage lavas also have positive anomalies of Ba and negative anomalies of Zr-Hf (Fig. 3). Site O7 foidite lavas have the strongest enrichment of LILEs and Th-U and the strongest negative anomalies of high field strength elements (HFSEs, e.g., Nb-Zr-Hf-Ti) (Fig. 3). These rejuvenated stage lavas show systematically lower SiO_2 and Al_2O_3 and higher total iron and CaO/Al_2O_3 compared to shield stage lavas (Fig. 2, Supplementary Fig. 2). Rejuvenated stage lavas also have systematically lower Ni than those of shield stage for a given MgO content (Fig. 2b). Moreover, rejuvenated stage lavas have overall higher CaO and MnO contents than those of shield stage for a given MgO content (Fig. 2 b&d).

3.3.2 *In situ* olivine and spinel chemistry

Olivine phenocrysts and olivine-spinel pairs have been analyzed for high-precision major and trace element compositions by EMPA, and the results are shown in Supplementary Table 3&4, respectively. The volcanic rock samples of shield and rejuvenated stages in this study have similar ranges in Fo# (molar Mg/(Mg+Fe)×100%) (Fig. 4). For shield stage volcanic rocks, the highest Fo#s of olivines are 86.8, 89.1, 88.5 and 87.4 for Waimea, Wai'anae, Ko'olau and Wailuku volcanics, respectively; while for rejuvenated stage volcanic rocks, the highest Fo#s of olivines are 87.5, 86.9, 87.3 and 84.1 for Koloa, Honolulu, Hana and Kula, respectively. As shown in Fig. 4, at a given Fo, shield stage volcanic rocks have olivine Ni contents distinctly

higher and Mn-Ca contents lower than those of global MORBs. The olivines of rejuvenated stage lavas also have Ni contents systematically higher than those of global MORBs but lower than those of shield stage lavas for a given Fo#. Despite the distinct compositions of olivine Ni between shield stage and rejuvenated stage lavas, their olivine Ca and Mn contents are comparable for a given Fo# (Fig. 4). The olivines with the highest Fo# for both shield and rejuvenated stages have similarly Mn and Ca contents, which are lower than those of MORBs.

4. Discussion

4.1 Implication of whole-rock geochemistry on the role of CO_2

It has been suggested that shield stage lavas characterized by depletion of CaO and enrichment of SiO_2 cannot be explained by melting of peridotites (Hauri, 1996; Wagner and Grove, 1998; Huang and Frey, 2005; Herzberg, 2006; Herzberg and Asimow, 2008; Dasgupta et al., 2010), but can be explained by partial melting of mixed pyroxenite (recycled oceanic crust) and peridotite (e.g., Sobolev et al., 2005&2007; Huang et al., 2007; Herzberg, 2011; Herzberg and Asimow, 2008; Jackson et al., 2012; Mallik and Dasgupta, 2012). Rejuvenated stage lavas are usually silica-undersaturated and enriched in CaO that are distinct from shield stage volcanism (Fig. 2). The enrichment of LREEs and LILEs in rejuvenated lavas (Fig. 3) could be explained by low degree of melting in the mantle source and a geochemically enriched mantle source. However, the high CaO and SiO_2-poor nature of rejuvenated stage lavas cannot be explained by melting of dry pyroxenite (e.g., Mallik and Dasgupta, 2013) or peridotite (e.g., Dasgupta et al., 2010) at any temperature and pressure. Results of high pressure/temperature experiments indicate that, with the presence of CO_2, partial melts of either peridotite or pyroxenite/eclogite have high CaO and low SiO_2 contents (e.g., Dasgupta et al., 2007; Mallik and Dasgupta, 2013).

Plate subduction is an effective way to introduce sedimentary carbonate into deep mantle (e.g., Zhang and Smith_Duque, 2014; Plank and Manning, 2019; but see also Thomson et al., 2016). If recycled oceanic crust is involved in the Hawaiian mantle plume, sedimentary carbonates may have played a role during mantle melting, especially at low degrees of melting. Based on the results of melting experiment (e.g., Mallik and Dasgupta, 2013), melting of carbonate-bearing MORB can only produce melts with MgO of <8 wt%, which cannot explain

Hawaiian rejuvenated stage lavas with MgO of >10 wt%. Partial melts of carbonated pyroxenite and peridotite mixture and carbonated peridotite have both high MgO and CaO contents, as well as low SiO_2 content (e.g., Mallik and Dasgupta, 2013). Carbonatitic melts typically have high contents of CaO, MnO, Ba, and REEs, and are depleted in high field strength elements (HFSEs, such as Nb-Ta-Zr-Hf-Ti) (e.g., Hoernle et al., 2002; Dixon et al., 2008; Dalou et al., 2009;-Jones et al., 2013). We find that Site O7 samples from the Honolulu volcanics on Oahu Island, in addition to their anomalously high CaO-MnO and extremely low SiO_2, have highly enriched LREEs and relative depletion in Nb-Ta-Zr-Hf-Ti (Fig. 3). These observations could be explained by melting a carbonated mantle source.

4.2 Role of CO_2 indicated by olivine Ca-Mn

Hawaiian rejuvenated stage volcanic rocks have higher CaO and MnO contents for a given MgO content than shield stage lavas (Fig. 2), while their olivine Ca and Mn contents overlap at a given olivine Fo# (Fig. 4), reflecting a difference in partitioning of Ca-Mn between olivine/melt during the two volcanic stages. To better understand the partitioning of Ca-Mn between olivine/melt in Hawaiian lavas, we have calculated the partition coefficients of Ca and Mn between olivine/melt (Supplementary Table 5). Hawaiian lavas in this study, both shield and rejuvenated stages, have variable amount of olivine accumulation, and the samples with clinopyroxene accumulation are excluded. A mineral-melt pair in equilibrium is required before calculation of partition coefficient. Although primary melt composition can be calculated by assuming a Fo of ~91, the exact Ca content of the equilibrium primary olivine is not known. Most of the rejuvenated stage lavas have variable degrees of olivine accumulations, thus, a way to obtain olivine-melt pairs in equilibrium is to remove the accumulated olivines. Thus, in this way, we can obtain the exact Ca composition of olivine in equilibrium. Ten to twenty olivine grains with the highest Fo# and their average chemical compositions were used as the final equilibrium olivine (Supplementary Table 5). These final equilibrium olivines have Fo# of 84-87 for rejuvenated stage lavas and 83-89 for shield stage lavas. We have removed this average olivine composition step-by-step from the melt until the resulted melt was in equilibrium with the average olivine based on PRIMelt3 program (Herzberg and Asimow, 2015), in which a melt Fe^{2+}/Fe_{tot} is specified. The resulted equilibrium melt compositions are shown in Supplementary Table 5. The equilibrium melts calculated for rejuvenated stages lavas have MgO of 8-12 wt%,

while the equilibrium melts of shield stage have MgO of 10-14 wt%. It is clear that the calculated melts are not primary melts but evolved melts in equilibrium with the average olivines. We have calculated the partition coefficients of Ca and Mn between olivine/melt based on these olivine-melt pairs, which are shown in Supplementary Table 6 and plotted in Fig. 5. The calculated olivine/melt partition coefficients of Ca and Mn for rejuvenated stage samples are overall lower than those for shield stage for a given olivine Fo# and melt MgO content, despite these evolved melts have degassed to certain degrees.

There are several observations indicating that CO_2 has played an essential role in the activities of Hawaiian mantle plume. Sisson et al. (2009) argued that a carbonated garnet lherzolite source is required to produce the pre-shield basanite-nephelinite lavas at Kilauea. Barsanti et al (2009) showed that a suite of magmas of recent (1842-1844) Kilauea eruption contain 2-6 wt% CO_2, and attributed the high CO_2 contents to enrichment by magma degassing at low pressures. Based on the CO_2 emission rate and volcanic magma supply rate at Kilauea, Anderson and Poland (2017 Nature Geoscience 10, 2017) estimated 1 wt% CO_2 in the parental magma supplying Kilauea, which translates to 263 ppm C in their mantle source. This is consistent with the result of a recent work using melt inclusions. Tucker et al (2019) showed that parental magmas of Hawaii volcanos (Hualalai, Kilauea, Koolau, Loihi and Mauna Loa) have 0.39-1.0 wt% CO_2, and their mantle sources contain 380-480 ppm CO_2 that are at least a factor of ~4 more than the MORB mantle.. The negatively correlated Rb/Sr and $^{87}Sr/^{86}Sr$ in shield stage Mahukona lavas (Huang et al., 2009) and the light Ca isotope compositions in most shield stage Hawaiian lavas (Huang et al., 2011) may reflect a role of sedimentary carbonates in the Hawaiian mantle plume. Wirth and Rocholl (2003) reported nanocrystalline diamond in pyroxenite xenolith of Oahu Island, which may crystallize from rejuvenated stage magmas. Dixon et al. (2008) argued for a role of carbonatite metasomatism in the petrogenesis of Hawaiian rejuvenated stage lavas, requiring a CO_2 rich mantle source during the rejuvenated stage volcanism.

As shown in Fig. 2, partial melts of carbonated pyroxenites and carbonated peridotites have higher contents of CaO and MnO compared to those from CO_2-free peridotites and pyroxenites.. Garnet, Clinopyroxene (Cpx) and orthopyroxene (Opx) are important hosts for Ca and Mn during the mantle melting processes. The Cpx/melt partition coefficient of Mn (1.06-1.16) is

lower than that between garnet/melt (1-4.8), but higher than that between Opx/melt (0.66-1.05) (Le Roux, 2011; Herzburg et al., 2013; Shea and Foley, 2019). The presence of CO_2 in the mantle source would increase the stability of Opx relative to Cpx and garnet, thus, the carbonated melts are enriched in Ca and Mn. This is supported by the observation that natural carbonatites usually are enriched in Ca and Mn (e.g., Hoernle et al., 2002). To further investigate the effect of CO_2 on the partitioning of Ca-Mn in olivine, we have selected the results of a suite of high-quality experiments with resulted melts similar in composition to this study for comparison.

Dasgupta et al (2007) conducted partial melting experiments on "peridotite+CO_2", and Mallik and Dasgupta (2013) conducted melting experiment on "eclogite+peridotite+CO_2". These two studies obtained carbonated silicate melts with SiO_2 of 30-48 wt% and CaO of 7-25 wt%, which are comparable to the geochemistry of rejuvenated stage lavas. We also compared the Ca partition coefficients for Hawaiian lavas with the results of experiments that produced olivines equilibrium with dry silicate melts (Kogiso et al., 1998; Robinson et al., 1998; Mallik and Dasgupta, 2012; Matzen et al., 2013 & 2017). These experiments either produced silicate melts in equilibrium with olivine based on melting of peridotite (Robinson et al, 1998) and mixed peridotite+eclogite (Kogiso et al, 1998; Mallik and Dasgupta, 2012), or modeled crystallization of olivine from MORB-like melts (Matzen et al., 2013; Matzen et al., 2017). These experiments all produced dry silicate melts with SiO_2 of 45-53 wt% and CaO of 6-11 wt% that are similar to shield stage lavas and olivines with high precision Ca contents. We calculated the partition coefficient of Ca between olivine/melt based on the above experiment studies, and the results are plotted in Fig. 5.

To understand the effect of CO_2 on partitioning of Mn between olivine and melt, we have compared our results with Mallik and Dasgupta (2013) (melting of eclogite+peridotite+CO_2), Mallik and Dasgupta (2012) (melting of peridotite+eclogite), and Dasgupta et al (2007) (melting of peridotite). The calculated partition coefficient of Mn for olivine-carbonated melt and olivine-dry silicate melt are shown in Fig. 5. As shown in Fig. 5, the experimental partition coefficients of Ca-Mn between olivine and carbonated silicate melt are overall lower than those between olivine and dry silicate melt for a given Fo# and MgO content of melt. Rejuvenated stage foidite samples have the lowest $D_{Ca}^{Ol\text{-}melt}$ and $D_{Mn}^{Ol\text{-}melt}$ for a given Fo# and magma MgO,

while the basanites and alkali basalts have $D_{Ca}^{Ol\text{-}melt}$ and $D_{Mn}^{Ol\text{-}melt}$ intermediate between foidites and shield stage lavas (Fig. 5). $D_{Ca}^{Ol\text{-}melt}$ and $D_{Mn}^{Ol\text{-}melt}$ from the olivine-dry silicate melt pairs are similar to those of shield stage lavas, while the partition coefficients of Ca-Mn calculated from the olivine/carbonated silicate melt are comparable to those of rejuvenated stage (Fig. 5). We suggest that the lower $D_{Ca}^{Ol\text{-}melt}$ and $D_{Mn}^{Ol\text{-}melt}$ of rejuvenated stage lavas relative to shield stage lavas are consistent with the role of CO_2 during the mantle melting.

The relationships of $D_{Ca}^{Ol\text{-}melt}$ vs. magma MgO for the shield and rejuvenated lavas in this study are compared with those resulted from experimental studies in Fig. 6a. As shown in Fig. 6a, the $D_{Ca}^{Ol\text{-}melt}$ for the dry silicate melt system first slightly decreases and then increases with decreasing MgO based on Gavrilenko et al (2016). The calculated $D_{Ca}^{Ol\text{-}melt}$ for shield stage lavas basically follow the trend in $D_{Ca}^{Ol\text{-}melt}$ vs. MgO for the dry silicate melts (Fig. 6a). Similar to the experimentally-derived $D_{Ca}^{Ol\text{-}melt}$ for carbonated silicate melt system, the $D_{Ca}^{Ol\text{-}melt}$ calculated for rejuvenated stage lavas are well below the curve for the dry silicate melts. We have calculated the difference in D_{Ca} ($\Delta D_{Ca}^{Ol\text{-}melt}$) between our calculated melts and experimental volatile-free melts, and the results are shown in Supplementary Table 6. The foidites with the lowest SiO_2 tend to have the lowest $D_{Ca}^{Ol\text{-}melt}$ and $D_{Mn}^{Ol\text{-}melt}$ for a given olivine Fo and melt MgO content (Fig. 5), while the basanites and alkali basalts are intermediate between foidites and shield stage lavas (Fig. 5). The overall high $\Delta D_{Ca}^{Ol\text{-}melt}$ for rejuvenated stage lavas relative to shield stage lavas (Fig. 6c) is consistent with the role of CO_2 in the mantle source, which significantly decreases SiO_2 in melt. Another role of CO_2 is to cause negative anomalies of high field strength elements (HFSEs) (e.g., decreases in Zr_N/Zr_N^*; N, normalized to primitive mantle; Zr_N^*, calculated as $\sqrt{Nd_N \times Sm_N}$), because REEs are enriched relative to HFSEs in carbonated melts (Zhang et al., 2017). As shown in Fig. 6d, the relatively low Zr_N/Zr_N^* (0.3 to 0.8) and elevated $\Delta D_{Ca}^{Ol\text{-}melt}$ for rejuvenated stage lavas relative to shield stage further indicates the role of CO_2 in mantle melting. It should be noted that the Honolulu foidites with the lowest SiO_2, and $D_{Ca}^{Ol\text{-}melt}$ and $D_{Mn}^{Ol\text{-}melt}$ have the strongest negative anomalies of Nb and Zr (Fig. 3, Fig. 6d). This suggests that rejuvenated stage foidites were subjected to the strongest influence of CO_2 during mantle melting.

Gavrilenko et al (2016) gave an equation of CO_2 (wt.%) = $270 \times \Delta D_{Ca} - 3330 \times \Delta D_{Ca}^2 + 1.8 \times 10^6 \times \Delta D_{Ca}^3$ to calculate melt CO_2 content based on the correlation of CO_2 with the difference

(ΔD_{Ca}) in the D_{Ca} values of carbonated melts and volatile-free melts. Since both H_2O and CO_2 can lower $D_{Ca}^{Ol\text{-}melt}$ (Gavrilenko et al., 2016), the effect of H_2O should also be considered to estimate magma CO_2 content based on $D_{Ca}^{Ol\text{-}melt}$. As shown in Dixon et al (1997), the alkali basaltic to nephelinitic lavas from the North Arch Volcanic Field, Hawaii, can have H_2O up to 1.9 wt% and CO_2 up to 5.4 wt% based on analyses of basalt glass and vesicles. Dixon et al (2008) further estimated 350 ppm H_2O in the Hawaii plume mantle, which is ~5 factors higher than the depleted MORB mantle. Dixon et al (2008) estimated a bulk partition coefficient of ~0.01 for H_2O in the Hawaiian mantle. Hawaiian rejuvenated lavas are usually considered to have partial melting extents of <5%, thus, we have calculated rejuvenated magma H_2O contents based on a bulk partition coefficient of 0.01 for H_2O and batch melting degrees of 2% and 4%, and our calculation results in H_2O contents of 1.17 wt% and 0.71 wt%, respectively. Shield stage magma H_2O is calculated by assuming a batch melting degree of 20% in Hawaiian mantle source, and a magma H_2O content of 0.17 wt% is obtained. For comparison, Hauri (2002 Chem Geol 183, 115-141) reported 0.03 to 0.84 wt % H_2O in melt inclusions from five shield stage lavas from Hawaii. We estimated the influence of H_2O on $D_{Ca}^{Ol\text{-}melt}$ (ΔD_{Ca} at a given H_2O content) based on Gavrilenko et al (2016). Then, we calculated the difference between $\Delta D_{Ca}^{Ol\text{-}melt}$ and ΔD_{Ca} at a given H_2O content, which is used to calculate the content of CO_2 based on the equation of Gavrilenko et al (2016). The calculated results of CO_2 are shown in Supplementary Table 6.

The mantle-derived primary magmas usually crystallize olivines with Fo# up to ~91, which are higher than the olivine phenocrysts in this study (Fig. 4). Thus, the result using the above method only represents the CO_2 concentration of evolved magmas, rather than primary magmas. The primary magma composition can be obtained by addition of equilibrium olivines to melt, however, the Ca contents of high Fo# (>90) olivines in equilibrium with primary magmas are not known. Therefore, we cannot obtain the primary magma CO_2 content directly based on the equation of Gavrilenko et al (2016). To obtain primary magma CO_2 content, we assume that magmas have not significantly degassed during fractionation. Then, the equilibrium olivines were added step by step to melts until the melts are in equilibrium with olivine with Fo# of 91 based on PREMELT3 MEGA.XLSM of Herzberg and Asimow (2015), the resulted primary magma compositions and fraction of olivine added are shown in Supplementary Table 6. The primary magma CO_2 contents were obtained after correction to fraction of olivine added to melts.

353 The calculation procedure and results are shown in Supplementary Table 6. The CO_2 contents of
354 the calculated shield stage primary magmas are close to zero. The calculated primary magma
355 CO_2 for rejuvenated stage are up to 5.6 wt% and 8.3 wt% for batch melting degrees of 2% and
356 4%, respectively (Supplementary Table 6).

357 We have compared our primary magma CO_2 contents with those calculated based on a
358 constant CO_2/Ba ratio. Because CO_2 is similar to Ba in incompatibility during mantle melting
359 (e.g., Anderson and Poland, 2017; Miller et al., 2019), the primary magma CO_2 content can be
360 estimated if the mantle source CO_2/Ba ratio can be determined. As suggested by previous studies
361 the Hawaiian mantle has a CO_2/Ba ratio of ~86 (Anderson and Poland, 2017). The calculated
362 primary magma CO_2 contents through this method is also shown in Supplementary Table 6. The
363 calculated primary magma CO_2 contents are 0.45 to 3.15 wt% for the shield stage, while the
364 primary magma CO_2 contents are 2.8 to 10 wt% for rejuvenated stage. We have plotted the
365 primary magma CO_2 contents for anhydrous melting and a melting degree of 4% in this study
366 with those based on the constant CO_2/Ba of 86 in Fig. 7. As shown in Fig. 7, the foidite samples
367 tend to have the highest primary magma CO_2 contents, while the basanites and alkali basalts are
368 similarly low relative to the foidite samples. The results of anhydrous melting are overall close to
369 those based on assuming a constant CO_2/Ba ratio, however, the results of hydrous melting,
370 melting degree of 4%, for rejuvenated stage are generally lower than those based on assuming a
371 constant CO_2/Ba ratio. Since the latter method is independent of uncertainties in magma
372 degassing and melting degrees, the lower primary magma CO_2 contents could have been caused
373 by these uncertainties. Despite discrepancy between the two methods, they are overall consistent
374 in resulting in primary magma CO_2 contents up to ~10 wt% for rejuvenated stage lavas and low
375 CO_2 contents for shield stage lavas, suggesting rejuvenated stage lavas have a similar source CO_2
376 to the plume mantle. However, as a constant CO_2/Ba ratio of Hawaiian mantle source is not
377 verified for shield and rejuvenated stage lavas, our work provides an independent constraint on
378 CO_2 enrichment in Hawaiian rejuvenated lavas.

379 **4.3 Olivine Ni: effects of source vs. temperature**

380 There are different views on the origin of Hawaiian rejuvenated stage volcanism, either
381 from the shallow metasomatized mantle lithosphere (Chen and Frey, 1983; Yang et al., 2003;
382 Bianco, 2005; Garcia et al., 2010), the deep mantle plume component (Frey et al., 2005; Dixon et

al., 2008; Sisson et al., 2009; Hofmann and Farnetani, 2013; DeFelice et al., 2019; Harrison et al., 2020), or both (Beguelin et al., 2019). The deep plume origin for rejuvenated stage melts is supported by their distinct isotopic compositions from the Pacific MORBs (Supplementary Fig. 3). Despite enrichment of LILEs and LREEs in rejuvenated stage lavas, they generally have more depleted isotopic compositions compared to shield stage lavas (Yang et al., 2003; Hofmann and Farnetani, 2013; Beguelin et al., 2019; DeFelice et al., 2019; Harrison et al., 2020). As shown in Supplementary Fig. 3, such a depleted signature cannot be explained by involvement of Pacific-type depleted upper mantle, but likely to have been derived from an intrinsic mantle plume component. However, it remains unclear how the low-degree melts of rejuvenated stage preferentially sample the isotopically depleted component in the mantle plume (Ribe and Christensen, 1999; Bianco and Ito, 2008; Beguelin et al. 2019; DeFelice et al. 2019). For example, it was suggested that rejuvenated stage lavas originated from a deep isotopically depleted zone separated from the primary melting zone that formed shield stage lavas (Ribe and Christensen, 1999), or from a depleted periphery of a zoned mantle plume (Bianco and Ito, 2008).

As shown in Fig. 4a, the olivine Ni contents of rejuvenated stage lavas are overall lower than those of shield stage, but higher than the global MORBs for a given olivine Fo#. In contrast, rejuvenated stage lavas have whole-rock Ni lower than shield stage lavas for a given MgO content (Fig. 2c). Increasing magma total alkaline (Na_2O+K_2O) increases the partition coefficient of Ni in olivine when total alkaline > 8 wt% (Förster et al., 2018). Most of our studied rocks have K_2O+Na_2O contents significantly lower than 8 wt%, hence, it is unexpected to have notable difference in $D_{Ni}^{Ol\text{-}melt}$ between shield and rejuvenated stage lavas. As we discussed above, CO_2 played a key role in the origin of rejuvenated stage magmatism. However, Girnis et al (2013) showed that CO_2 have negligible influence on the partitioning of Ni between olivine/melt. As such, we suggest the relatively lower olivine Ni contents of the rejuvenated stage compared with the shield stage reflects a lower Ni content in their parental magmas, as indicated by whole-rock Ni contents (Fig. 2c).

Melting temperature/pressure, source lithology, and source Ni content could influence primary magma Ni content (Sobolev et al., 2005&2007; Putirka et al, 2011; Matzen et al., 2013). Partial melts of eclogite/pyroxenite react with peridotite in the Hawaii mantle plume to convert

413 olivines to Opx and to form stage-2 pyroxenite with a lower proportion of (or no) olivine in the
414 source (Sobolev et al., 2005&2007). Thus, the mantle source with a lowered olivine proportion
415 would generate primary melts with elevated Ni (Sobolev et al., 2005). As indicated by Matzen et
416 al (2013, 2017), $D_{Ni}^{Ol\text{-}melt}$ increases with decreasing temperature and pressure, thus, elevated
417 source temperatures and pressures would result in an increase of olivine Ni in Hawaiian shield
418 lavas. In addition to the stage-2 pyroxenite in the mantle source, the higher olivine Ni of
419 Hawaiian shield stage lavas may at least partly have been caused by higher melting temperatures
420 and pressures (e.g., Matzen et al., 2013). Thus, evaluation of difference in primary magma
421 temperatures among the shield stage lavas, rejuvenated stage lavas and normal MORBs would
422 help understand the origin of their Fo-Ni systematics (Fig. 4a).

423 In this study, we have calculated the magma temperatures of shield and rejuvenated stages
424 based on the olivine-spinel aluminum exchange thermometry. This thermometry is advantageous
425 over the olivine-liquid thermometry since it is independent of equilibrium pressure and melt
426 compositions. Details on the use of the olivine-spinel aluminum exchange thermometry are
427 referred to Wan et al (2008) and Coogan et al (2014). We selected the volcanic rock samples
428 from the rejuvenated and shield stages that contain the highest olivine Fo#. We used the equation
429 given by Coogan et al (2014) ($T(K)=10000/(0.575+0.884Cr\#-0.897\ln(Al_2O_3^{Ol}/Al_2O_3^{Sp}))$), which
430 has extended the use of this thermometry to a relatively oxidizing environment. The data of
431 olivine-spinel are filtered based on the requirements of Coogan et al (2014), i.e., Cr# between
432 0-69%, and Fe^{3+}/Total FeO <35%. The calculated results are shown in Supplementary Table 4
433 and plotted in Fig. 8a. As shown in Fig. 8a, shield stage olivines with the highest Fo# (~89) tend
434 to have the highest crystallization temperatures. Rejuvenated stage olivines have statistically
435 lower crystallization temperatures and Fo# than those of shield stage as shown in Fig. 8 c-d. The
436 slightly lower olivine crystallization temperatures of rejuvenated stage lavas could also be
437 indicated by their slightly higher olivine Al_2O_3 (Supplementary Fig. 4) (Coogan et al., 2014).
438 However, the lavas of both shield and rejuvenated stages approximately follow the trend of melt
439 temperature vs. equilibrium olivine Fo# of the Icelandic primary magmas as shown in Herzberg
440 and Asimow (2015). Thus, for the given highest olivine Fo# (e.g., ~91), broadly similar primary
441 magma temperatures for the shield and rejuvenated stage lavas are expected (Fig. 8). As shown
442 in Fig. 8a, at the highest Fo# of up to 91, the MORB olivines tend to have lower temperatures

compared with those of Hawaiian olivines. This indicates that the Hawaiian primary magmas, both shield and rejuvenated stages, crystallized high Fo# olivines at higher temperatures than those of normal MORBs.

Since Hawaiian shield and rejuvenated stage lavas show different Sr-Nd-Hf isotopic compositions (Supplementary Fig. 3; Yang et al., 2003; Hofmann and Farnetani, 2013; DeFelice et al., 2019), the overall lower olivine Ni contents of rejuvenated stage lavas relative to those of shield stage may reflect a mantle source effect. As shown in Fig. 8, high Fo olivines from both shield and rejuvenated stage lavas have similar crystallization temperatures. The effect of melting-crystallization temperature difference (Matzen et al., 2013) may have not contributed significantly to the observed olivine Ni difference.

The mantle source of Hawaiian shield stage lavas has been considered to contain eclogites that were most likely derived from ancient recycled oceanic crust. Subducted altered oceanic crust, as an important carrier of secondary carbonates (Zhang and Smith_Duque, 2014), may constitute a source of CO_2 in the Hawaiian mantle plume. Thus, it is possible that CO_2-bearing mixed eclogite/peridotite exists in the Hawaii mantle plume. However, because the plume mantle source has melted to high degrees to form shield stage lavas, most of CO_2 would be extracted from the source mantle after high degrees of melting. As CO_2 is highly incompatible during mantle melting (e.g., Dixon et al., 2008), the resulted refractory residual mantle after extraction of shield stage lavas would be difficult to produce carbonated melts. Because Hawaiian rejuvenated stage lavas were formed 0.5-2 Myr after shield stage and ~100 km from the plume axis, it is possible that the rejuvenated lavas were sourced from the edge of the mantle plume, where mantle upwelling and decompression rate are lower than the plume axis (Fig. 9).

As indicated by this study, the rejuvenated stage lavas were most likely sourced from carbonated peridotites that are intrinsic to the Hawaiian mantle plume. Thus, the mantle plume peridotites may have experienced metasomatism of low degree carbonated melts. This is consistent with the enriched trace element patterns and negative anomalies of HFSEs in rejuvenated lavas (Fig. 3). However, the distinct Sr-Nd-Hf isotopic compositions between rejuvenated and shield stage lavas indicate that such carbonated melts were unlikely derived from a CO_2-bearing eclogite/pyroxenite (carbonate-bearing recycled oceanic crust) feeding shield stage lavas. A possible source for the carbonated melts in the mantle plume is subducted

lithospheric mantle (e.g., Kelemen and Manning, 2015). Although carbonate precipitation is generally considered to occur mainly in the oceanic crust during seafloor alteration, it would also occur in shallow lithospheric mantle of the bending plate before subduction (Kelemen and Manning, 2015), and in the exposed abyssal peridotites as represented by slow- to ultra-slow spreading ridge settings (e.g., Dick et al., 2000; Schroeder et al., 2002). These carbonate-bearing subducted peridotites may constitute the source required by Hawaiian rejuvenated stage lavas. As shown in Fig. 9, the low degree carbonated melts of such carbonate-bearing peridotites near the plume edge can metasomatize the mantle plume peridotites. Thus, along with the upwelling of mantle plume, such carbonated peridotites would decompress and melt, which may explain the CO_2-rich rejuvenated stage lavas.

5 Conclusions

The origin of Hawaiian rejuvenated stage magmatism remains a subject of debate. In this study, we have analyzed the whole-rock major and trace elements, *in situ* high-precision geochemistry of olivines and olivine-spinel pairs of Hawaiian rejuvenated and shield stage lavas. Unlike shield stage, rejuvenated stage lavas with anomalously high CaO and low SiO_2 and negative anomalies of HFSEs, which could be explained by the influence of CO_2 in the source. It is notable that the olivine Ni contents of rejuvenated stage lavas are systematically lower than those of shield stage, but higher than normal MORBs for a given olivine Fo#. While rejuvenated stage lavas have whole-rock CaO and MnO higher than shield stage, their olivine Ca and Mn contents are similar to each other for a given Fo#. Our study results in that $D_{Ca}^{Ol\text{-}melt}$ and $D_{Mn}^{Ol\text{-}melt}$ for rejuvenated stage lavas are systematically lower than those of shield stage, which we suggest is caused by the influence of CO_2. Our calculation based on the reduced $D_{Ca}^{Ol\text{-}melt}$ relative to dry basaltic melts indicates that rejuvenated stage primary melts were rich in CO_2, while shield stage melts were relatively dry (low volatile contents). The temperatures of primary magmas of rejuvenated stage are similar to the shield stage, but systematically higher than normal primary MORB magmas. The relatively low olivine Ni of rejuvenated lavas compared to shield stage can be attributed to the mantle source lithology dominated by peridotites, rather than stage-2 pyroxenite in shield stage mantle source. It is suggested that rejuvenated stage lavas were originated from the melting of carbonated peridotites in the Hawaiian mantle plume.

Acknowledgments

We thank Claude Herzberg, Jacqueline Dixon, Daniel Heaton and Eemu Ranta for their comments and constructive suggestions. JunHua Guo is thanked for the help on rock sampling. This work was financially supported by the National Natural Science Foundation of China (Nos. 41876040, 91858206, 41888101), the Laboratory for Marine Geology, Qingdao National Laboratory for Marine Science and Technology (No. MGQNLM-TD201806), and Taishan Scholars Program of Shandong Province (No. tsqn201909157).

Data Availability Statement

Data archiving is underway, and will be deposited in Mendeley Data after the manuscript is accepted. A copy of our data for review purpose is uploaded as Supplementary Information.

References

Anderson, K.R., Poland, M.P., 2017. Abundant carbon in the mantle beneath Hawai'i. Nature Geoscience, 10(9), 704-708.

Ballmer, M.D., Ito, G., van Hunen, J., Tackley, P.J., 2011. Spatial and temporal variability in Hawaiian hotspot volcanism induced by small-scale convection, Nature Geoscience, 4, 457–460.

Barsanti, M., Papale, P., Barbato, D., Moretti, R., Boschi, E., Hauri, E., Longo, A., 2009. Heterogeneous large total CO_2 abundance in the shallow magmatic system of Kilauea volcano, Hawaii. Journal of Geophysical Research-Solid Earth, 114.

Batanova, V.G., Thompson, J.M., Danyushevsky, L.V., Portnyagin, M.V., Garbe-Schönberg, D., Hauri, E., Kimura, J.I., Chang, Q., Senda, R., Goemann, K. and Chauvel, C., 2019. New olivine reference material for in situ microanalysis. Geostandards and Geoanalytical Research, 43(3): 453-473.

Béguelin, P., Bizimis, M., McIntosh, E.C., Cousens, B., Clague, D.A., 2019. Sources vs processes: Unraveling the compositional heterogeneity of rejuvenated-type Hawaiian magmas. Earth and Planetary Science Letters, 514, 119-129.

Borisova, A.Y., Tilhac, R., 2021. Derivation of Hawaiian rejuvenated magmas from deep carbonated mantle sources: A review of experimental and natural constraints. Earth-Science

Reviews, 222, 103819.

Chauvel, C., McDonough, W., Guille, G., Maury, R., Duncan, R., 1997. Contrasting old and young volcanism in Rurutu Island, Austral chain, Chemical Geology, 139, 125-143.

Chen, C.Y. Frey, F.A., 1983. Origin of Hawaiian tholeiite and alkalic basalt. Nature, 302 (5911), 785-789.

Clague, D.A. Dalrymple, G.B., 1987. The Hawaiian-Emperor volcanic chain. part I. Geologic evolution. Volcanism in Hawaii, 1 (1350), 5-54.

Coogan, L.A., Saunders, A.D., Wilson, R.N., 2014. Aluminum-in-olivine thermometry of primitive basalts: Evidence of an anomalously hot mantle source for large igneous provinces. Chemical Geology, 368, 1-10.

Dalou, C., Koga, K. T., Hammouda, T., Poitrasson, F., 2009. Trace element partitioning between carbonatitic melts and mantle transition zone minerals: implications for the source of carbonatites. Geochimica Cosmochimica Acta, 73, 239-255.

Dasgupta R, Hirschmann, M.M., 2010. The deep carbon cycle and melting in Earth's interior. Earth and Planetary Science Letters, 298, 1–13.

Dasgupta, R., Hirschmann, M.M., Smith, N.D., 2007a. Water follows carbon: CO_2 incites deep silicate melting and dehydration beneath mid-ocean ridges. Geology 35(2), 135–138.

Dasgupta, R., Hirschmann, M.M., Smith, N.D., 2007b. Partial Melting Experiments of Peridotite + CO_2 at 3 GPa and Genesis of Alkalic Ocean Island Basalts. Journal of Petrology 48, 2093-2124.

Dasgupta, R., Jackson, M.G., Lee, C.-T.A., 2010. Major element chemistry of ocean island basalts-conditions of mantle melting and heterogeneity of mantle source. Earth and Planetary Science Letters, 289, 377-392.

Dasgupta, R., Hirschmann, M.M., Stalker, K., 2006. Immiscible transition from carbonate-rich to silicate-rich melts in the 3 GPa melting interval of eclogite plus CO_2 and genesis of silica-undersaturated ocean island lavas. Journal of Petrology, 47(4): 647-671.

DeFelice, C., S. Mallick, Saal, A.E., Huang, S., 2019. An isotopically depleted lower mantle component is intrinsic to the Hawaiian mantle plume. Nature Geoscience, 12 (6): 487-495.

Dick, H. J., Natland, J. H., Alt, J. C., Bach, W., Bideau, D., Gee, J. S., et al., 2000. A long in situ section of the lower ocean crust: results of ODP Leg 176 drilling at the Southwest Indian

561 Ridge. Earth and planetary science letters, 179(1), 31-51.
562 Dixon, J.E., Clague, D.A, Wallace, P., Poreda, R., 1997. Volatiles in alkalic basalts form the
563 North Arch Volcanic Field, Hawaii: extensive degassing of deep submarine-erupted alkalic
564 series lavas. Journal of Petrology, 38 (7): 911-939.
565 Dixon, J., Clague, D.A. Cousens, B. Monsalve, M.L., Uhl, J., 2008. Carbonatite and silicate melt
566 metasomatism of the mantle surrounding the Hawaiian plume: Evidence from volatiles, trace
567 elements, and radiogenic isotopes in rejuvenated-stage lavas from Niihau, Hawaii.
568 Geochemistry Geophysics Geosystems, 9 (9). Doi:10.1029/2008GC002076.
569 Forster, M. W., D. Prelevic, H. R. Schmuck, S. Buhre, H. R. Marschall, R. Mertz-Kraus and D. E.
570 Jacob (2018). Melting phlogopite-rich MARID: Lamproites and the role of alkalis in
571 olivine-liquid Ni-partitioning. Chemical Geology, 476: 429-440.
572 French, S.W., Romanowicz, B., 2015. Broad plumes rooted at the base of the Earth's mantle
573 beneath major hotspots. Nature, 525 (7567), 95–99.
574 Frey, F.A., Clague, D., Mahoney, J.J., Sinton, J.M., 2000. Volcanism at the edge of the Hawaiian
575 plume: petrogenesis of submarine alkalic lavas from the North Arch volcanic field. Journal of
576 Petrology, 41(5), 667-691.
577 Garcia, M.O., Swinnard, L., Weis, D., Greene, A.R., Tagami, T., Sano, H., Gandy, C.E., 2010.
578 Petrology, Geochemistry and Geochronology of Kaua'i Lavas over 4•5 Myr: Implications for
579 the Origin of Rejuvenated Volcanism and the Evolution of the Hawaiian Plume. Journal of
580 Petrology, 51(7), 1507-1540.
581 Gerbode, C., Dasgupta, R., 2010. Carbonate-fluxed melting of MORB-like pyroxenite at 2.9 GPa
582 and genesis of HIMU ocean island basalts. Geophysical Research Letters 51, 2067-2088.
583 Gavrilenko, M., Herzberg, C., Vidito, C., Carr, M.J., Tenner, T., and Ozerov, A., 2016. A
584 Calcium-in-Olivine Geohygrometer and its Application to Subduction Zone Magmatism.
585 Journal of Petrology 57(9): 1811–1832.
586 Gervasoni, F., Klemme, S., Rohrbach, A., Grutzner, T., Berndt, J., 2017. Experimental
587 constraints on mantle metasomatism caused by silicate and carbonate melts. Lithos, 282: 173–
588 186.
589 Girnis, A.V., Bulatov, V.K., Brey, G.P., Gerdes, A., Hofer, H.E., 2013. Trace element partitioning
590 between mantle minerals and silico-carbonate melts at 6-12 GPa and applications to mantle

591 metasomatism and kimberlite genesis. Lithos, 160, 183–200.
592 Hammouda, T., Chantel, J., Devidal, J.L., 2010. Apatite solubility in carbonatitic liquids and
593 trace element partitioning between apatite and carbonatite at high pressure. Geochimica et
594 Cosmochimica Acta, 74, 7220–7235.
595 Harrison, L.N., Weis, D. and Garcia, M.O., 2020. The multiple depleted mantle components in
596 the Hawaiian-Emperor chain. Chemical Geology, 532, 119324.
597 Hauri, E.H., 1996. Major-element variability in the Hawaiian mantle plume. Nature, 382(6590),
598 415-419.
599 Herzberg, C., 2006. Petrology and thermal structure of the Hawaiian plume from Mauna Kea
600 volcano. Nature, 444 (7119), 605-609.
601 Herzberg, C., Asimow, P.D., 2008. Petrology of some oceanic island basalts: PRIMELT2. XLS
602 software for primary magma calculation. Geochemistry Geophysics Geosystems, 9(9).
603 Herzberg, C., 2011. Identification of source lithology in the Hawaiian and Canary Islands:
604 Implications for origins. Journal of Petrology, 52(1), 113–146.
605 Herzberg, C., Asimow, P.D., Ionov, D.A., Vidito, C., Jackson, M.G., Geist, D., 2013. Nickel and
606 helium evidence for melt above the core–mantle boundary. Nature, 493(7432), 393-397.
607 Herzberg, C., Asimow, P.D., 2015. PRIMELT 3 MEGA. XLSM software for primary magma
608 calculation: peridotite primary magma MgO contents from the liquidus to the solidus.
609 Geochemistry Geophysics Geosystems, 16(2), 563–578.
610 Hirose, K., 1997. Partial melt compositions of carbonated peridotite at 3 GPa and role of CO_2 in
611 alkali-basalt magma generation. Geophysical Research Letters 24, 2837–2840.
612 Hoernle, K., Tilton, G., Le Bas, M.J., Garbe-Schönberg, D., 2002. Geochemistry of oceanic
613 carbonatites compared with continental carbonatites: mantle recycling of oceanic crustal
614 carbonate. Contrib. Mineralolgy and Petrology, 142, 520–542.
615 Hofmann, A. W., Farnetani, C.G., 2013. Two views of Hawaiian plume structure, Geochemistry
616 Geophysics Geosystem, 14, 5308–5322.
617 Hofmann, A.W., 1997. Mantle geochemistry: the message from oceanic volcanism. Nature, 385,
618 219–229.
619 Huang, S., Abouchami, W., Blichert-Toft, J., Clague, D.A., Cousens, B.L., Frey, F.A., Humayun,
620 M., 2009. Ancient carbonate sedimentary signature in the Hawaiian plume: Evidence from

621 Mahukona volcano, Hawaii, Geochemistry Geophysics Geosystem, 10, Q08002,
622 doi:10.1029/2009GC002418.
623 Huang, S., Frey, F.A., Blichert-Toft, J., Fodor, R.V., Bauer, G.R., Xu, G., 2005. Enriched
624 components in the Hawaiian plume: evidence from Kahoolawe Volcano, Hawaii.
625 Geochemistry Geophysics Geosystems, 6(11).
626 Huang, S. C., Hall, P.S., Jackson, M.G., 2011, Geochemical zoning of volcanic chains associated
627 with Pacific hotspots, Nature Geoscience, 4, 874–878, doi:10.1038/NGEO1263.
628 Huang, S., Humayun, M., Frey, F.A., 2007. Iron/manganese ratio and manganese content in
629 shield lavas from Ko'olau Volcano, Hawai'i. Geochimica et Cosmochimica Acta, 71(18),
630 4557-4569.
631 Jones, A.P., Genge, M., Carmody, L., 2013. Carbonate Melts and Carbonatites. Reviews in
632 Mineralogy and Geochemistry, 75: 289–322.
633 Kiseeva, E. S. et al., 2012. An experimental study of carbonated eclogite at 3.5–5.5 GPa:
634 Implications for silicate and carbonate metasomatism in the cratonic mantle. Journal of
635 Petrology 53, 727–759.
636 Kiseeva, E. S., Litasov, K. D., Yaxley, G. M., Ohtani, E., Kamenetsky, V. S., 2013. Melting and
637 phase relations of carbonated eclogite at 9–21 GPa and the petrogenesis of alkali-rich melts in
638 the deep mantle. Journal of Petrology 54, 1555–1583.
639 Kelemen, P.B., Manning, C.E., 2015. Reevaluating carbon fluxes in subduction zones, what goes
640 down, mostly comes up. Proceedings of the National Academy of Sciences, 112(30),
641 E3997-E4006.
642 Kogiso, T., Hirose K., Eiichi, T., 1998. Melting experiments on homogeneous mixtures of
643 peridotite and basalt: application to the genesis of ocean island basalts. Earth and Planetary
644 Science Letters, 162, 45–61.
645 Le Roux, V., Dasgupta, R., Lee, C.T.A., 2011. Mineralogical heterogeneities in the Earth's
646 mantle: Constraints from Mn, Co, Ni and Zn partitioning during partial melting. Earth and
647 Planetary Science Letters, 307 (3-4): 395-408.
648 Mallik, A., Dasgupta, R., 2013. Reactive infiltration of MORB-eclogite-derived carbonated
649 silicate melt into fertile peridotite at 3 GPa and genesis of alkalic magmas. Journal of
650 Petrology 54, 2267-2300.

651 Mallik, A., Dasgupta, R., 2012. Reaction between MORB-eclogite derived melts and fertile
652 peridotite and generation of ocean island basalts. Earth and Planetary Science Letters, 329:
653 97–108.
654 Matzen, A. K., M. B. Baker, J. R. Beckett and E. M. Stolper (2013). The Temperature and
655 Pressure Dependence of Nickel Partitioning between Olivine and Silicate Melt. Journal of
656 Petrology 54(12): 2521-2545.
657 Matzen, A. K., Baker, M.B., Beckett, J.R., Wood, B.J., Stolper, E.M., 2017. The effect of liquid
658 composition on the partitioning of Ni between olivine and silicate melt. Contribution to
659 Mineralogy and Petrology, 172(1): 3.
660 Miller, W.G., Maclennan, J., Shorttle, O., Gaetani, G.A., Le Roux, V., Klein, F., 2019. Estimating
661 the carbon content of the deep mantle with Icelandic melt inclusions. Earth and Planetary
662 Science Letters, 523, 115699.
663 Montelli, R., Nolet, G., Dahlen, F.A., Masters, G., Engdahl, E.R., Hung, S.H., 2004.
664 Finite-frequency tomography reveals a variety of plumes in the mantle. Science, 303 (5656),
665 338-343.
666 Phillips, E. H., K. W. W. Sims, D. R. Sherrod, V. J. M. Salters, J. Blusztajn and H. Dulai (2016).
667 Isotopic constraints on the genesis and evolution of basanitic lavas at Haleakala, Island of
668 Maui, Hawaii. Geochimica et Cosmochimica Acta, 195: 201-225.
669 Plank, T., Manning, C.E., 2019. Subducting carbon. Nature, 574 (7778), 343-352.
670 Qi, L., Hu, J., Gregoire, D.C., 2000. Determination of trace elements in granites by inductively
671 coupled plasma mass spectrometry. Talanta 51, 507–513.
672 Reiners, P.W., Nelson, B.K., 1998. Temporal-compositional-isotopic trends in rejuvenated stage
673 magmas of Kauai, Hawaii, and implications for mantle melting processes. Geochimica et
674 Cosmochimica Acta, 62, 13, 2347–2368.
675 Robinson, J.A.C., Wood, B.J., Blundy, J.D., 1998. The beginning of melting of fertile and
676 depleted peridotite at 1.5 GPa. Earth and Planetary Science Letters, 155, 97–111.
677 Schroeder, T., John, B., Frost, B.R., 2002. Geologic implications of seawater circulation through
678 peridotite exposed at slow-spreading mid-ocean ridges. Geology, 30(4): 367-370.
679 Shea, J.J., Foley, S.F., 2019. Evidence for a Carbonatite-Influenced Source Assemblage for
680 Intraplate Basalts from the Buckland Volcanic Province, Queensland, Australia. Minerals, 9

(9), 546.

Sherrod, D.R., Nishimitsu, Y., and Tagami, T., 2003, New K–Ar ages and the geologic evidence against rejuvenatedstage volcanism at Haleakalā, East Maui, a postshield-stage volcano of the Hawaiian island chain: Geological Society of America Bulletin, 115 (6), 683–694.

Sherrod, D.R., Sinton, J.M., Watkins, S.E., Brunt, K.M., 2007. Geologic Map of the State of Hawaii. Open-File Report 2007–1089. U.S. Geological Survey, Reston, Virginia 2007.

Sisson, T.W., Kimura, J.I., Coombs, M.L., 2009. Basanite–nephelinite suite from early Kilauea: carbonated melts of phlogopite–garnet peridotite at Hawaii's leading magmatic edge. Contributions to Mineralogy and Petrology, 158(6): 803-829.

Sobolev, A.V., Hofmann, A.W., Kuzmin, D.V., Yaxley, G.M., Arndt, N.T., Chung, S.L., Danyushevsky, L.V., Elliott, T., Frey, F.A., Garcia, M.O., Gurenko, A.A., Kamenetsky, V.S., Kerr, A.C., Krivolutskaya, N.A., Matvienkov, V.V., Nikogosian, I.K., Rocholl, A., Sigurdsson, I.A., Sushchevskaya, N.M., Teklay, M., 2007. The amount of recycled crust in sources of mantle-derived melts. Science 316, 412-417.

Sobolev, A.V., Hofmann, A.W., Sobolev, S.V., Nikogosian, I.K., 2005. An olivine-free mantle source of Hawaiian shield basalts. Nature 434, 590-597.

Tucker, J.M., Hauri, E.H., Pietruszka, A.J., Garcia, M.O., Marske, J.P., Trusdell, F.A., 2019. A high carbon content of the Hawaiian mantle from olivine-hosted melt inclusions. Geochimica et Cosmochimica Acta 254: 156-172.

Wagner, T.P., Grove, T.L. 1998. Melt/harzburgite reaction in the petrogenesis of tholeiitic magma from Kilauea volcano, Hawaii. Contributions to Mineralogy and Petrology, 131(1), 1-12.

Weis, D., Garcia, M.O., Rhodes, J.M., Jellinek, M., Scoates, J.S., 2011. Role of the deep mantle in generating the compositional asymmetry of the Hawaiian mantle plume, Nature Geoscience, 4, 831–838, doi:10.1038/NGEO1328.

Wirth, R., Rocholl, A., 2003. Nanocrystalline diamond from the Earth's mantle underneath Hawaii. Earth and Planetary Science Letters, 211 (3-4), 357-369.

Yang, H.J., Frey, F.A., Clague, D.A., 2003. Constraints on the source components of lavas forming the Hawaiian North Arch and Honolulu Volcanics, Journal of Petrology, 44, 603–627.

Zhang, G.L., Chen, L.H., Jackson, M.G., Hofmann, A.W., 2017. Evolution of carbonated melt to

711 alkali basalt in the South China Sea. Nature Geoscience. 10(3), 229-235.
712 Zhang, G.L., Smith_Duque C, 2014. Seafloor basalt alteration and chemical change in the ultra
713 thinly sedimented South Pacific. Geochemistry Geophysics Geosystems, DOI:
714 10.1002/2013GC005141.
715 Zhang, G.L., Zhang, J., Wang, S., Zhao, J.X., 2020. Geochemical and chronological constraints
716 on the mantle plume origin of the Caroline Plateau. Chemical Geology, doi.org/10.1016/
717 j.chemgeo.2020.119566.
718

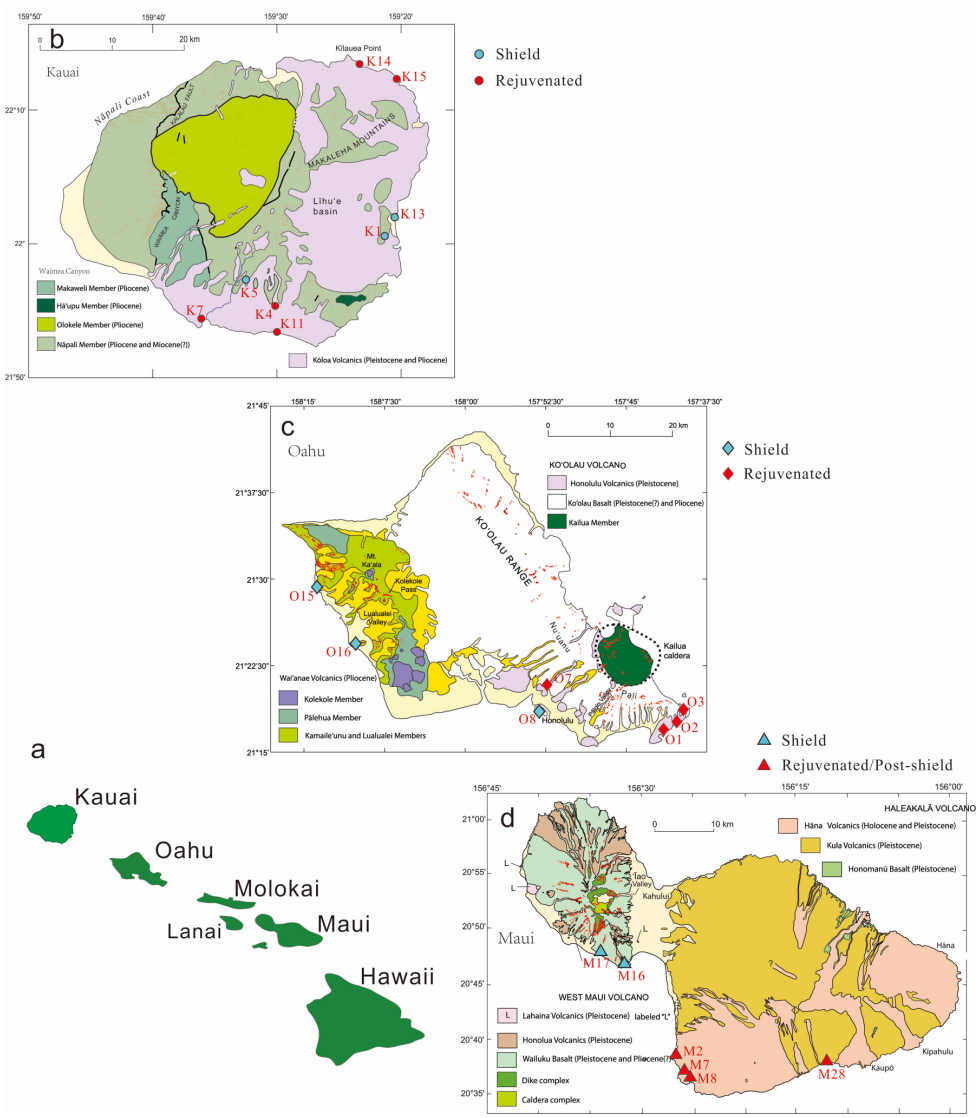

719

720 **Figure 1**. Geological setting and sampling locations of this study. The geologic maps are
721 modified according to Sherrod et al (2007).
722

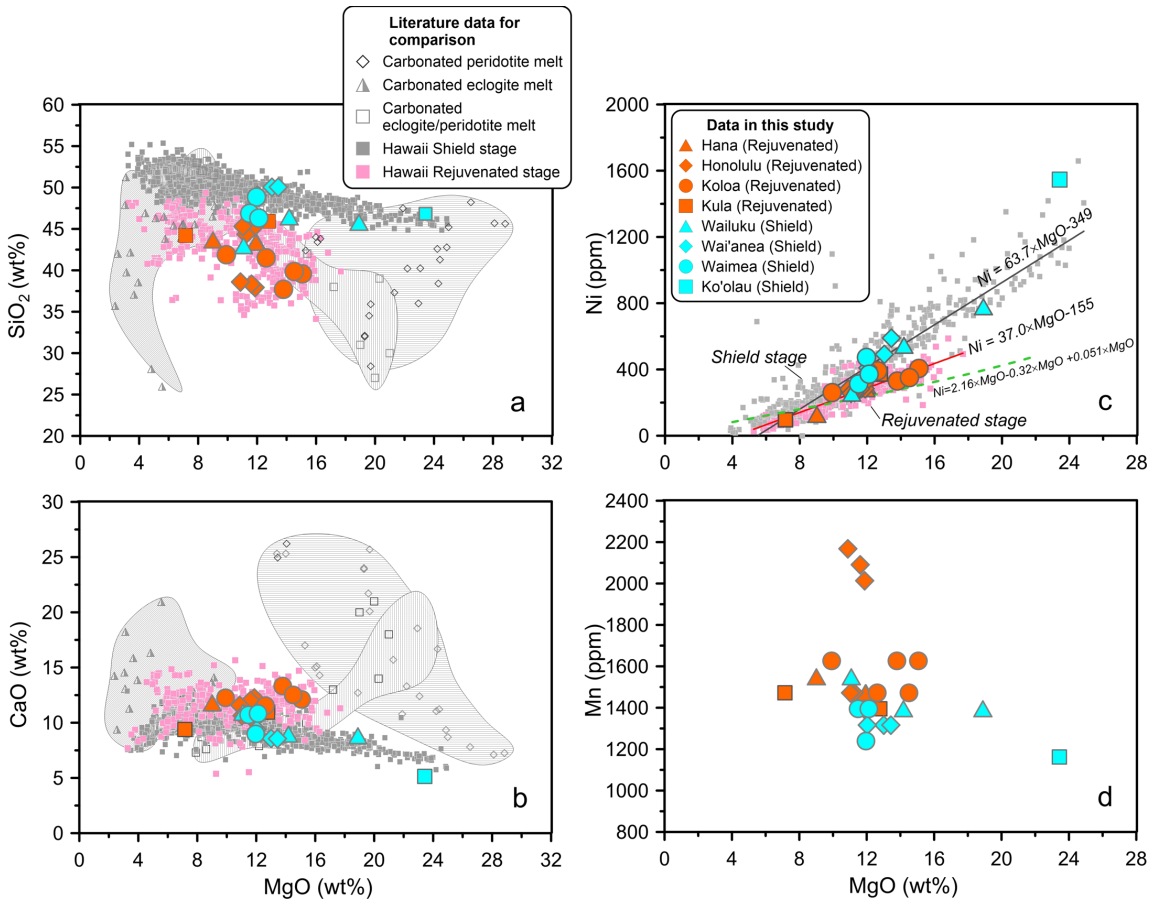

723

724 **Figure 2. Plots of bulk-rock MgO vs. (a) SiO_2, (b) CaO, (c) Ni and (d) Mn for volcanic rocks**
725 **of Hawaiian islands**. Green dashed line in (c), primary accumulated fractional melts of fertile
726 mantle peridotite (KR-4003) modeled by calculated by Herzburg (2011). Source of literature
727 data for comparison: Carbonated peridotite melt (Hirose, 1997; Dasgupta et al., 2007),
728 carbonated eclogite melt (Kiseeva et al., 2012; Kiseeva et al., 2013; Hammouda et al., 2010;
729 Gerbode and Dasgupta, 2010), carbonated eclogite+peridotite melt (Mallik and Dasgupta,
730 2013), data of Hawaiian shield and rejuvenated stage in (*a*)-(*c*) for comparison are from
731 http://georoc.mpch-mainz.gwdg.de/georoc/Entry.html.

732

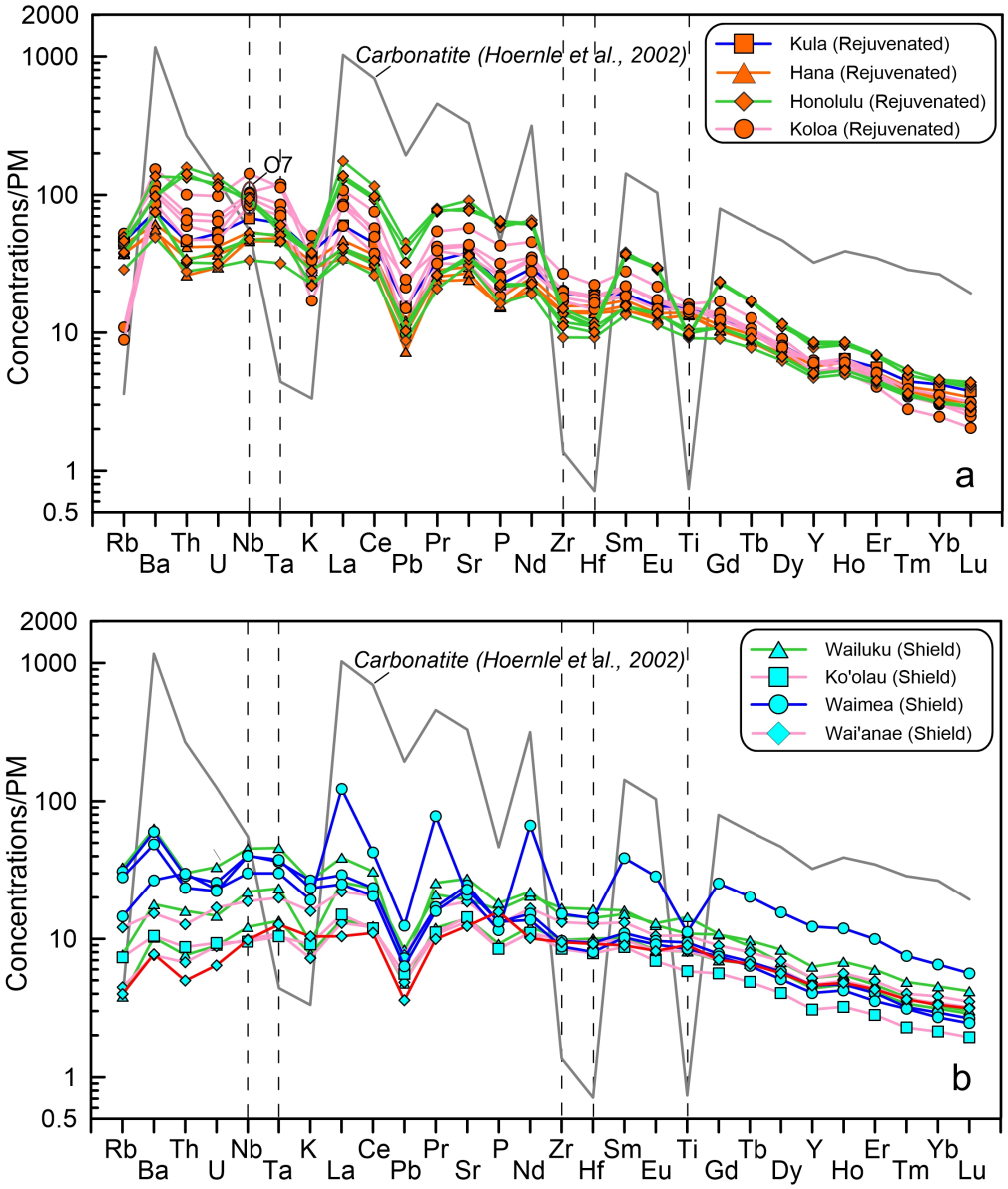

Figure 3. **Trace element patterns for the volcanic rock samples from Hawaiian Islands**. Data are normalized to the primitive mantle data of McDonough and Sun (1995). The typical carbonatite (Sample #: 85LB25, the carbonatite lava) for comparison from Hoernle et al (2002).

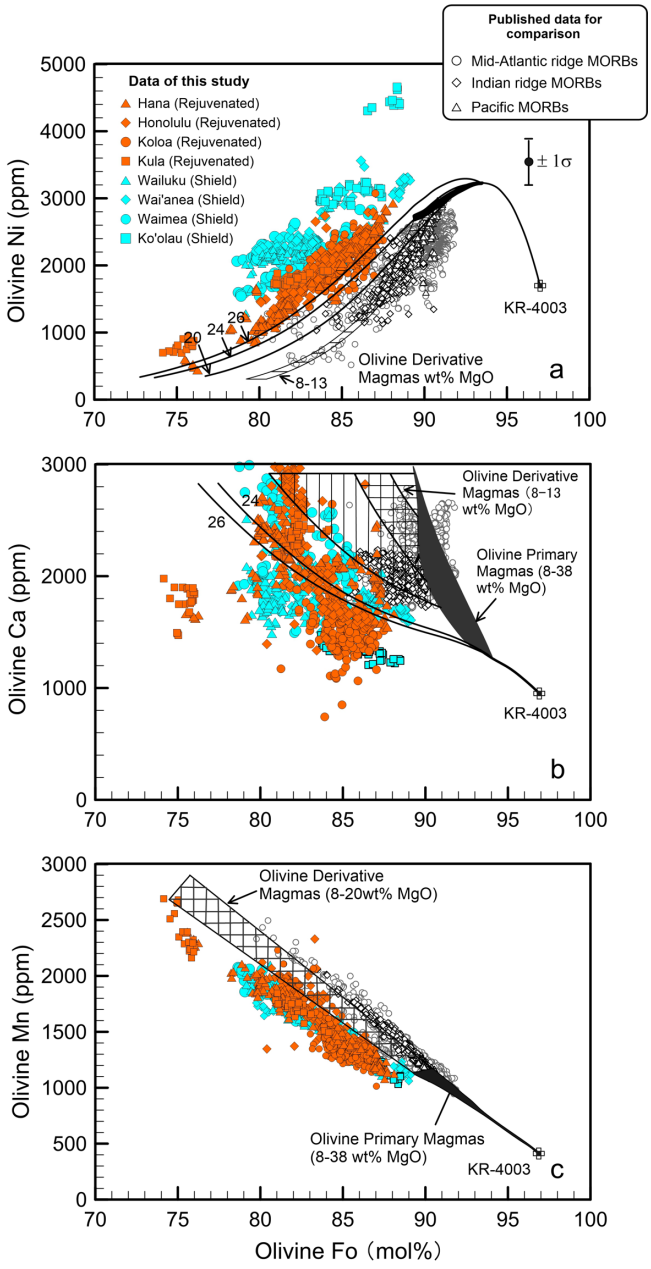

739

740 **Figure 4**. **Plots of olivine Mg number (Fo) vs. (a) Ni, (b) Ca and (c) Mn**. The calculated
741 olivine compositions are based on Herzberg (2011). Black area shows the olivines of primary
742 magmas (MgO of 8–38 wt%) from fertile peridotite KR-4003 with 1964 ppm Ni, 3.45 wt%
743 CaO, 1007 ppm Mn, and 8.02 wt% FeO. Numbered lines in (a) and (b) are calculated olivines
744 of olivine-fractionated derivative magmas, and the numbers indicate the MgO contents of
745 olivine derivative magmas. Short lines with end-bars in (a) and (d) are ±1σ Ni and Fe/Mn
746 variations of the primary magmas from which olivines crystallize. Data of olivine for global
747 MORBs (Indian ridge, Mid-Atlantic Ridge, and East Pacific Rise) and Hawaiian OIBs are
748 from Sobolev et al. (2007).

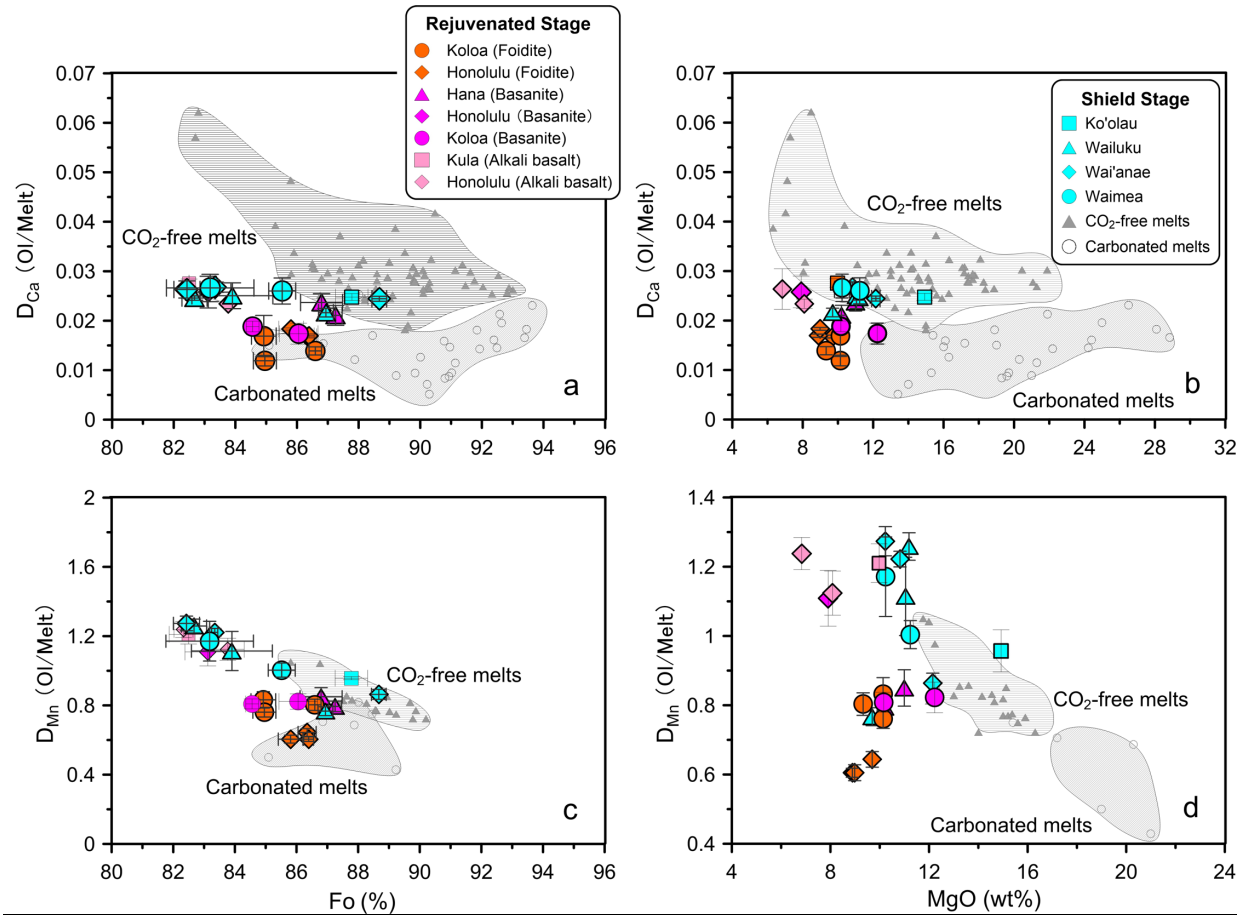

749

750 **Figure 5. Plots of D_{Ca} (Ol/melt) vs. (a) Fo and (b) melt MgO, and D_{Mn} (Ol/melt) vs. (c)**
751 **olivine Mg number (Fo) and (d) melt MgO.** Source of literature data for comparison: data
752 for D_{Mn} (Mallik and Dasgupta, 2012 & 2013; Matzen et al., 2017), data for D_{Ca} (Mallik and
753 Dasgupta, 2012 & 2013; Matzen et al., 2017; Dasgupta et al., 2007; Robinson et al., 1998;
754 Kogiso et al., 1998).

755

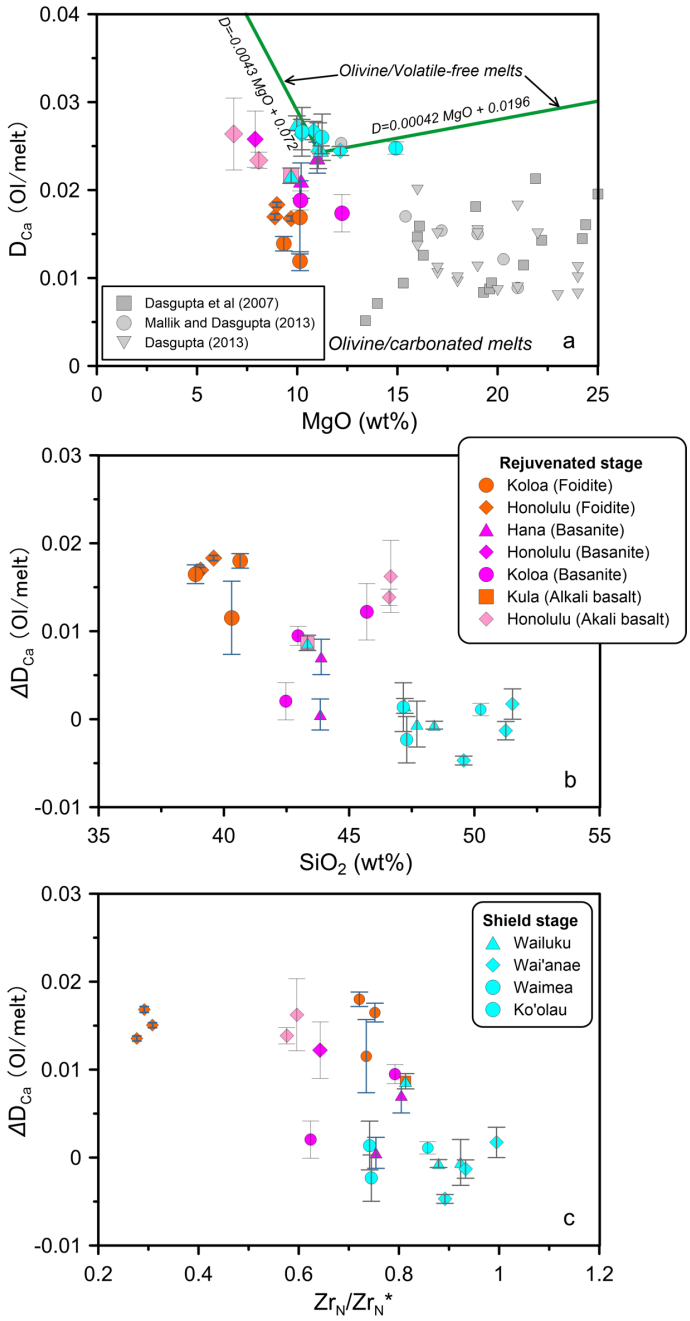

Figure 6. Plots of (a) $D_{Ca}^{Ol/melt}$ vs. equilibrium melt MgO, $\Delta D_{Ca}^{Ol/melt}$ vs. (b) SiO_2 and (c) Zr_N/Zr_N^*. The results of high-pressure/temperature experiments from Dasgupta et al. (2007, 2013) and Mallik and Dasgupta (2013) are plotted in (a) for comparison. The green solid line in (a) indicates the results of such experiments with volatile-free melts from Gavrilenko et al. (2016). $\Delta D_{Ca}^{Ol/melt}$ indicates difference between the olivine D_{Ca} values of calculated melts and volatile-free melts. Zr_N, normalized to primitive mantle data of McDonough and Sun (1995). Zr_N^*, calculated as square root of $Nd_N \times Sm_N$.

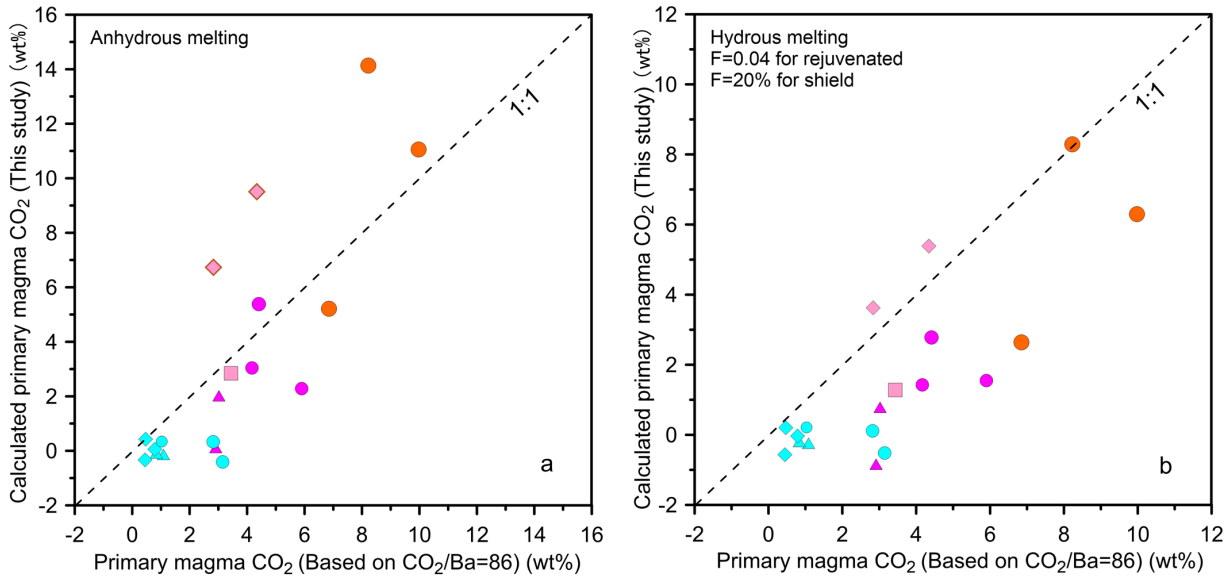

765

766 **Figure 7. Plots of calculated primary magma CO_2 based on CO_2/Ba=86 vs. calculated**
767 **primary magma CO_2 on basis of (a) anhydrous and (b) hydrous melting**. Anhydrous
768 meting assumes no influence of water on partition of Ca in olivine. F, melting degree of
769 mantle based on which water content is calculated. Primary magma CO_2 content is calculated
770 based on CO_2/Ba=86 and is corrected based on fraction of olivine added during primary
771 magma calculation.

772

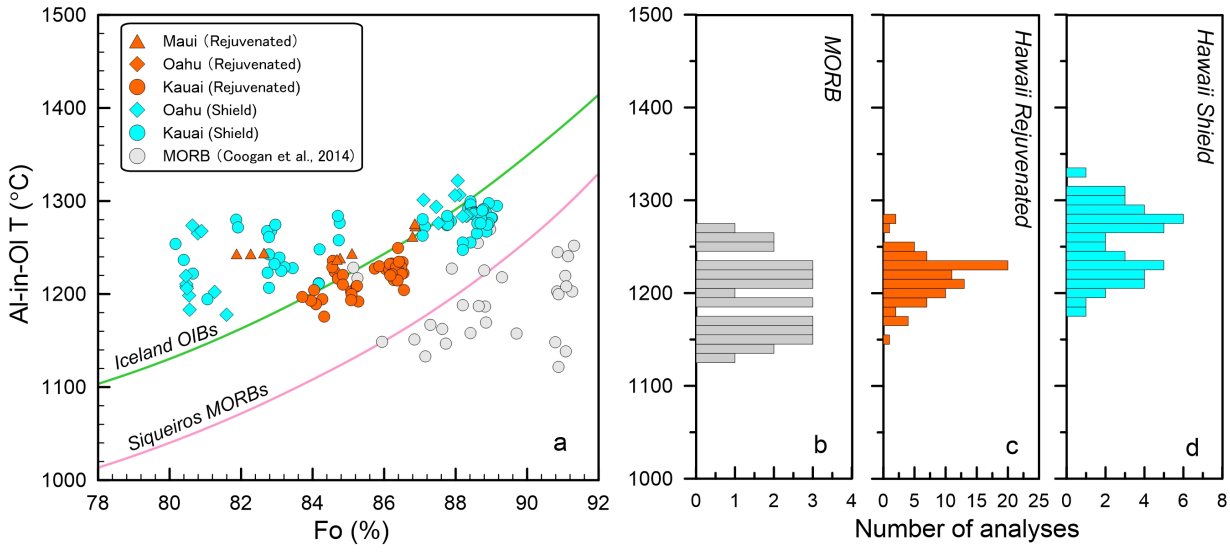

773

774 **Figure 8. Al-in-olivine crystallization temperature as a function of olivine Fo (a) and**
775 **histogram for comparing Hawaii rejuvenated and shield stage crystallization**
776 **temperature (b-c)**. Data of MORB temperature for comparison are from Coogan et al (2014).
777 The solid lines for Iceland OIB and Siqueiros MORB are calculated by PREMELT3
778 MEGA.XLSM based on Herzberg and Asimow (2015).

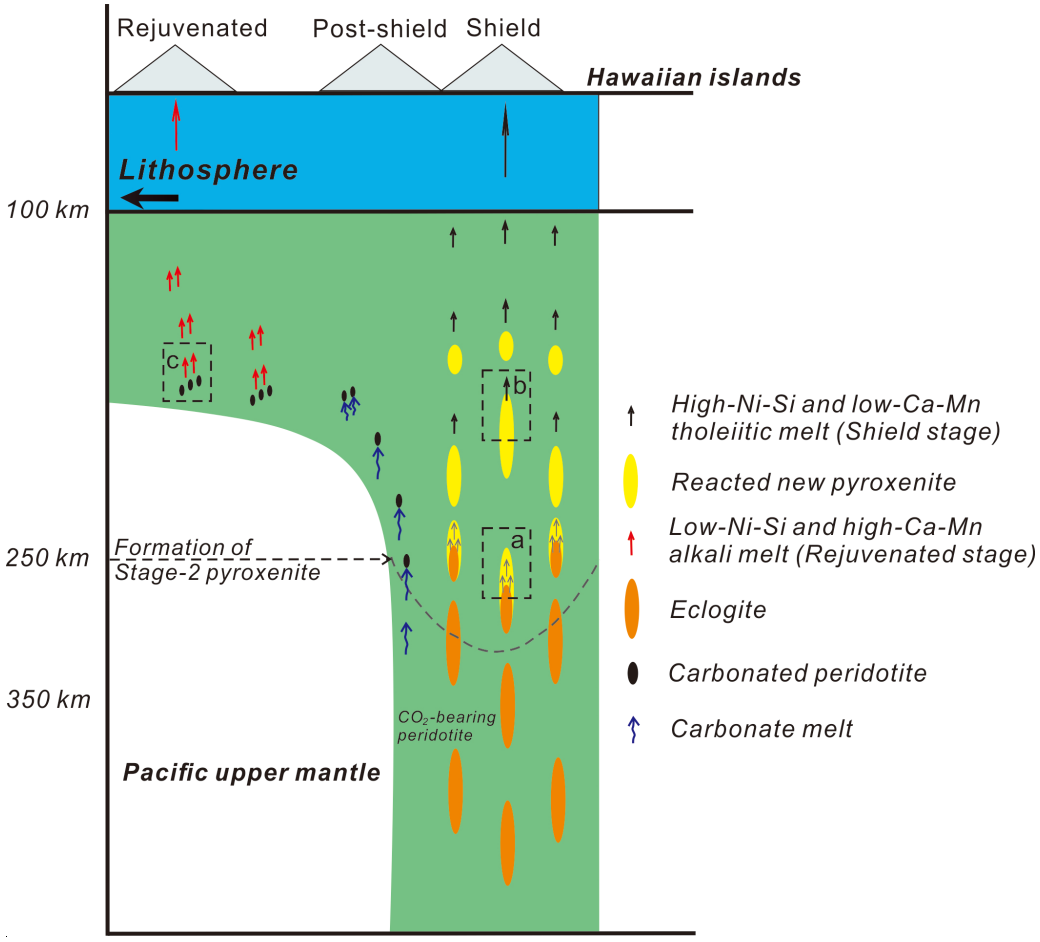

Figure 9. Model showing genesis of shield stage and rejuvenated stage volcanism. *a.* Reaction of eclogite melt with peridotite to form Stage-2 pyroxenite (Sobolev et al., 2005); *b.* High-degree melt of stage-2 pyroxenite to produce Hawaii Shield stage volcanism; *c.* Melting of carbonated peridotite to form CO_2-rich rejuvenated stage melts.